Supporting Information

Nanoscale Clustering of the Neurotrophin Receptor TrkB Revealed by Super-resolution STED Microscopy

Borislav Angelov[a] and Angelina Angelova[b,*]

[a]Institute of Physics, ELI Beamlines, Academy of Sciences of the Czech Republic, Na Slovance 2, CZ-18221 Prague, Czech Republic,

[b]Institut Galien Paris-Sud, CNRS UMR 8612, Univ. Paris-Sud, Université Paris-Saclay, LabEx LERMIT, F-92290 Châtenay-Malabry cedex, France

* Corresponding author: angelina.angelova@u-psud.fr

I. Materials and methods

1. Chemicals

Cis-4,7,10,13,16,19-docosahexaenoic acid (DHA), bovine serum albumin, retinoic acid, paraformaldehyde, and NH_4Cl were supplied by *Sigma*. Human recombinant brain-derived neurotrophic factor (BDNF) protein and a high affinity monoclonal antibody against the human TrkB receptor (MAB 397, mouse IgG2b) were purchased from *Bio-Techne* (*R&D Systems*). Biotium CF488A Goat anti-mouse IgG2b (γ2b) antibody was received from *Ozyme*. Anti-TrkB (extracellular)-ATTO-488 antibody was purchased from *Alomone Labs*. Phosphate buffered saline (PBS), Dulbeccos's Modified Eagle Medium (DMEM), fetal bovine serum (FBS), trypsin, and antibiotics (penicillin/streptomycin) were supplied by *Lonza* and *Life Technologies*. Cell fixation buffers and reagents were purchased from *Bio-Techne.* DMSO and absolute ethanol were obtained from *Carlo Erba*. Water was purified by a Milli-Q apparatus (*Millipore Corp.*).

2. Cell culture

The human neuroblastoma SH-SY5Y cell line (Géral *et al*., 2012) was grown in sterile plastic flasks (Nunclon^{TM} surface, NUNC Corp.) in DMEM medium with high glucose content and supplementation with antibiotics (penicillin/streptomycin), pH 7.4, and 10% fetal bovine serum (FBS) in 5% CO_2 environment at 37 ^{o}C. The experiments were performed with cell cultures on passages ranging from 9 to 12. A neuronal cell phenotype was induced by treatment with FBS-containing medium enriched with 10 µM retinoic acid (RA) during 5 days (Encinas *et al.*, *J. Neurochem.* 2000). Washing of the differentiated neuron-like cells and subsequent treatment with 10 µM RA in the lack of FBS caused a degeneration process. It was associated with cell body collapse over time and lost of neurite outgrowth in the absence of trophic factor support. Formulations containing neurotrophin BDNF (5 ng/mL) as well as BDNF and ω-3 polyunsaturated fatty acid (50 nM DHA) induced neuronal survival and regeneration. The effect of DHA on the TrkB receptor distribution was studied by super-resolution microscopy after 72h incubation of the cell line with formulations representing therapeutic treatment conditions (Scheme 1). The selection of the neuroprotective compositions, concentrations, and incubation times for the imaging study was done based on the recently established *in vitro* biological effects (Guerzoni *et al*., *Pharm. Res.* 2017).

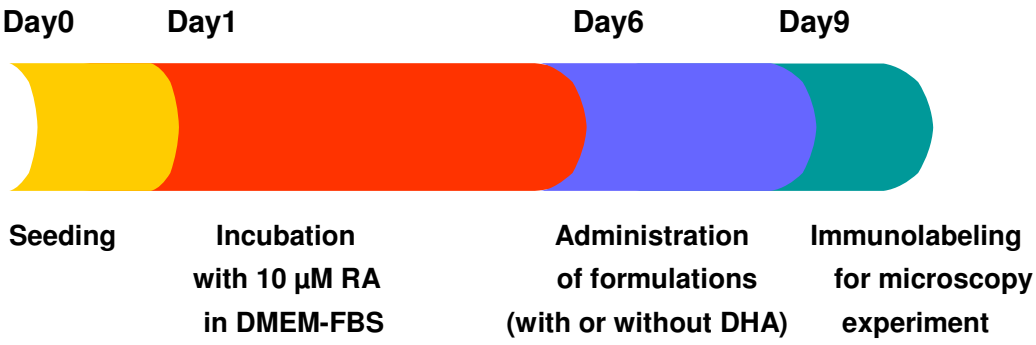

Scheme 1. Cell culture treatment scheme for generation of a neuronally-derived SH-SY5Y human neuroblastoma cells expressing the tropomyosin-related kinase (TrkB) receptor. The exposure to 10 µM RA was followed by incubation with neuroregenerative formulations of BDNF (5 ng/mL) with or without 50 nM DHA (in the lack of serum) prior to immunolabelling and cell fixation for fluorescence microscopy.

3. Sample preparation methodology

The SH-SY5Y cells were detached by trypsin from the growth flasks, counted, and seeded on glass cover slits in 12-well or 6-well culture plates. The initial cell density was from 60,000 (for 12-well) to 200,000 cells per well (for 6-well plates). High-precision coverslit glasses No. 1.5H with a thickness of 0.170 mm ± 0.005 mm and a diameter 12 mm (*Marienfeld*) were used for the STED microscopy investigation. The cell differentiation occurred through treatment with retinoic acid during 5 days, which stimulated the expression of the tropomyosin-related kinase (TrkB) receptor. Formulations of neurotrophin BDNF and polyunsaturated fatty acid DHA were prepared in serum-free DMEM medium by dilution of stock solutions of the reagents. The concentration of BDNF was 5 ng/ml and that of DHA was 50 nM. Prior treatment of the neuronal cell phenotype, the medium was aspirated and the cells were rinsed with serum-free DMEM. The immunostaining for microscopy imaging was performed 72 hours after administration of the formulations. The experimental design is shown in Scheme 1.

Immunostaining of the TrkB receptor molecules expressed on the surface of the studied cells was done following a fixation protocol accomplished at room temperature. The medium was removed from the glass cover slits and the culture was washed by PBS. Then, the cells were fixed in 4% paraformaldehyde fixation buffer for 15 min, incubated with 50 mM NH_4Cl solution for 10 min, and washed twice in PBS at room temperature. Incubation with a blocking buffer (2% BSA in PBS) was applied for 30 min. After washing by PBS, the high-affinity monoclonal anti-h-TrkB antibody, recognizing the extracellular domain of the membrane receptor, was incubated with the cells at a concentration 10 μg/ml during one hour. This concentration corresponded to a saturation of the receptor sites. The excess monoclonal antibody was washed after incubation.

The fluorescently labelled (CF™488A) secondary antibody was handled according to the manufacturer's specification. The advantage of the employed Biotium CF™488A antibody conjugate is that it is highly photostable and biologically more specific with regard to antibodies labelled by Alexa Fluor® 488 or FITC dyes. Whereas the Alexa Fluor® 488 dye carries multiple negative charges, the CF™488A dye was minimally charged and was not expected to modify the isoelectric point of the labelled antibody. According to manufacturer, the CF™488A antibody conjugate ensures protein detection with high specificity and high signal-to-noise ratio. Dilution of 1/500 was applied for the Biotium CF™488A-labelled antibody, whereas the dilution of the high-affinity primary antibody was 1/50.

In control experiments for fluorescence detection upon excitation at a wavelength 488 nm, treated and non-treated RA-differentiated SH-SY5Y human cells were incubated with a

secondary antibody (CF™488A fluorescently labelled immunoglobulin) in the lack of a primary anti-TrkB antibody recognizing the protein receptor. For this purpose, the cells were incubated (after rinsing) with the secondary antibody (4 μg/ml in PBS) in dark for one hour. The imaging experiments demonstrated that the fluorescent antibody conjugate does not bind to the TrkB receptor itself, *i.e*. the non-specific adsorption was avoided.

The cover slit samples were washed twice with PBS and they were mounted on rectangular glass slides using Vectashield mounting medium. The samples were stored at 4°C prior to image acquisition and analysis. Experiments were performed also with a fluorescently labelled (ATTO-488) primary anti-TrkB antibody. In this case, the immunodetection was feasible but the photostability of the reagent was not optimal for nanoscopy experiments aiming at determination of the TrkB receptor distribution on the cell surface. Thus, the primary anti-h-TrkB antibody/secondary antibody (Biotium CF™488A conjugate) couple was employed for the STED nanoscopy imaging of fixed SH-SY5Y cells.

4. Microscopy imaging

Cellular morphologies of live cells were evaluated under inverted light microscope. Micrographs of the SH-SY5Y cells, seeded at a density 200,000 cells per well, were obtained using the DIC mode of the confocal microscope ZEISS (model LSM 510, Zeiss, Germany). The resolution of the confocal laser scanning microscope technique was about 200 nm. The DIC images served to detect the neurite loss or extension upon induction of the cellular neurodegeneration or neuroregeneration processes. The image visualization was done by the Zeiss LSM image browser. Neurite outgrowth and extension were observed in response to the neurotrophic treatments leading to neuronal survival and regeneration.

A commercial STED Nanoscope Leica TCS SP8-gated STED (*Leica* Microsystems), integrating a confocal laser scanning platform with high photon efficiency, was available at the "*Cellular Imaging*" platform of the Paris-Sud Institute of Therapeutic Innovation (IPSIT), Paris-Saclay University. Quantitative imaging was achieved through super-sensitive Leica HyD hybrid detector (GaAsP). The inverted microscope was operated with a STED oil objective of the HC PL APO 100x/1.40 OIL type. Enhanced lateral resolution of the gated STED imaging was achieved by a classical vortex donut, whereas the vertical resolution was optimized by a z-donut. Images were recorded in a Z-stack mode in order to identify the plane corresponding to the cell surface expression of the TrkB receptor. High-speed acquisition permitted to reduce the phototoxic effects. Greater imaging details were achieved through optimization of speed, resolution, and sensitivity parameters. The experimental resolution down to 23 nm was further increased by software magnification of the observed details. The *Image J* software and *Leica Application Suite* (LAS) (*Leica Microsystems*) were employed.

Image deconvolution by *Huygens* professional software helped to resolve the nanometric features below 20 nm.

The patterns of TrkB membrane receptor distribution were examined with immuno-fluorescently labelled neuronally-derived SH-SY5Y cells, which were seeded at a density of 80,000 cells per well. The microscopy imaging of fixed cells was performed at room temperature. A laser wavelength of 488 nm was used for excitation of the fluorophore. For STED, the depletion laser was set at a wavelength of 592 nm. The requirement of the STED method is that the wavelength of the depletion laser beam should be higher that that of the wavelength of the excitation laser beam. Control experiments with excitation at 488 nm were performed for verification of the level of the autofluorescence of the cells with regard to the fluorescence intensity of the studied fluorophore. For excitation at 488 nm, no fluorescence was detected upon incubation of the cells with a fluorescently-labelled secondary antibody in the absence of anti-h-TrkB primary antibody. The magnification of the objective was 100× (oil). These control experiments on non-specific adsorption of fluorescent molecules guaranteed that the detected fluorescence was due to specific recognition of the extracellular domain of the TrkB membrane protein.

Under the employed experimental conditions, the full size of the recorded confocal fluorescence images was 73.12 × 73.12 μm^2. The raw STED images were recorded with a scale of intensities from 0 to 255. For the selected area of the image shown in Fig. 4a, the micrographs were acquired with 23.2 × 23.2 μm^2 dimensions, which corresponded to pixel sizes of 22.68 nm × 22.68 nm. Several image areas were analyzed by *ImageJ* algorithms using additional digital magnification down to a pixel size of 5.67 nm × 5.67 nm in the *Huygens* deconvoluted software-magnified STED images. The performed digital zoom by *ImageJ* did not modify the detectable topological features. No interpolation of the TrkB receptor distribution was observed.

The area of a single pixel (5.67 nm × 5.67 nm) in the treated images corresponded to the projected area of a single TrkB receptor dimer after the performed software magnification by 4×. In this way, the detection capacity of the technique was enhanced for in-plane identification of individual membrane protein dimers (or couples of monomers). Regarding the fluorescence intensity, 256 intensity levels of the detector setup were feasible for detection. For nanometer size spots, the measured intensities were within the range of 12 levels (Fig. S4).

For fluorescent intensity analysis, the original STED images were deconvoluted by the *Huygens* professional software and were imported in *ImageJ* in the 8-bit format, which

corresponds to 256 gray levels of intensity. This procedure preserves the original 256 intensity levels of the STED detector. The size of the image pixel was equal to 22.68 nm based on the STED microscope calibration. Subsequently, an intensity threshold was adjusted to 4 in order to remove the dark background below this level. The images were zoomed 4 times. The algorithm built-up in *ImageJ* was used for the determination of the protein cluster sizes considering the applied intensity threshold. The performed zoom did not change the resolution of the gated STED method.

The cluster boundary determination was done thought the intensity threshold. We tested different threshold values from 0 to 18. Consistent results were obtained at an intensity level 4 and higher. Once we have determined the sizes of all clusters (particles) in the images, it was straightforward to obtain the shown statistical histograms by common mathematical procedures.

For further technical details we refer to the program user guide and the examples of image treatment available at https://imagej.nih.gov/ij/docs/guide/user-guide.pdf

A large number of intensity plots were used in order to create the statistical histogram shown in Fig. 6b. Various portions of super-resolution STED images were analyzed prior to obtain the representative statistical distribution of the protein nanoscale clustering. The analyzed number of single and nanoclustered pixels reached over 4 millions for areas with large protein clusters, yielding 205 levels of intensities. Examples of STED image portions containing empty pixels and pixels occupied by molecules are shown in Figs. S2 and S3.

Independent biological repeats of the cells were performed in triplicate. The experimental methodology was optimized as to yield reproducible results. Cellular assays were performed at least two times in order to evaluate the effects of auto-fluorescence, specificity of immunolabeling, measurement noise upon immunofluorescent detection, fluorophore degradation at increased laser irradiation, *etc*. For every treatment condition, five fields of cells were imaged at high magnification. The zoom was further performed at the single cell level in order to search for the maximal super-resolution upon the patterned illumination. Representative results are shown after examination of the cells treated in twelve well plates. The statistic analysis is presented in Figures5, 6b and Table S1.

II. Additional results

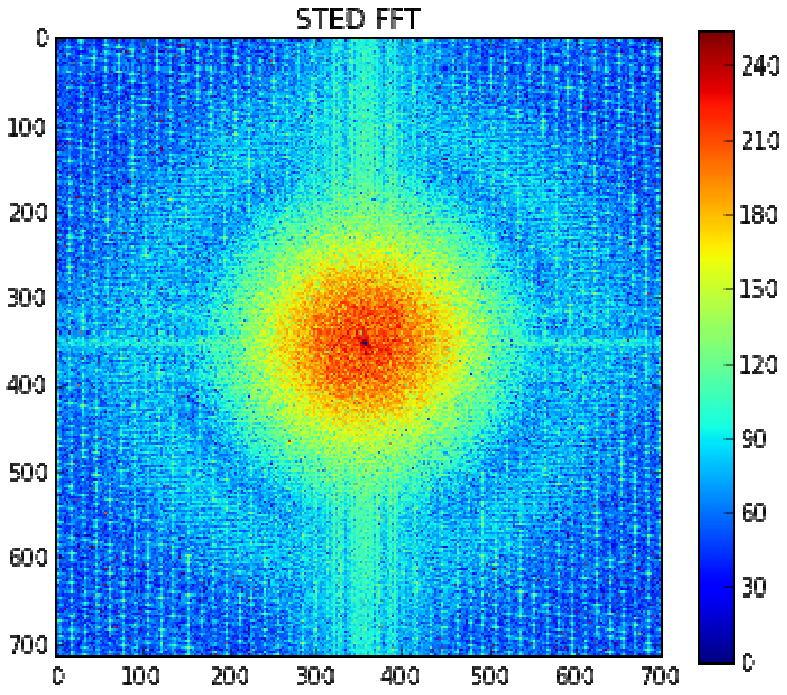

Figure S1. Fast Fourier Transform (FFT) of the STED image from Fig. 3c demonstrating the lack of long-range arrangement of the TrkB receptors into ordered crystalline domains in the neuronal lipid membranes.

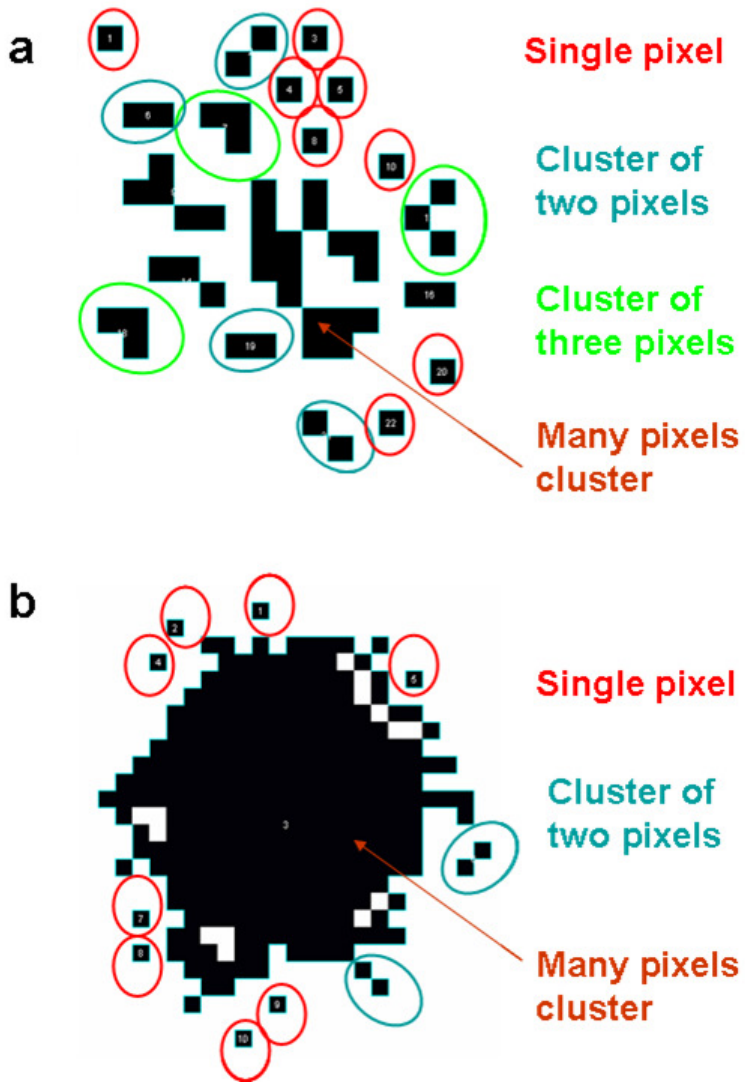

Figure S2. Distinction of single pixels *versus* cluster boundaries of connected pixels by application of the *ImageJ* software. Examples of formation of (a) small receptor clusters, and (b) a large cluster of oligomeric proteins. The pixel dimension is 5.67×5.67 nm^2 in the magnified portions of *Huygens* deconvoluted gated STED images.

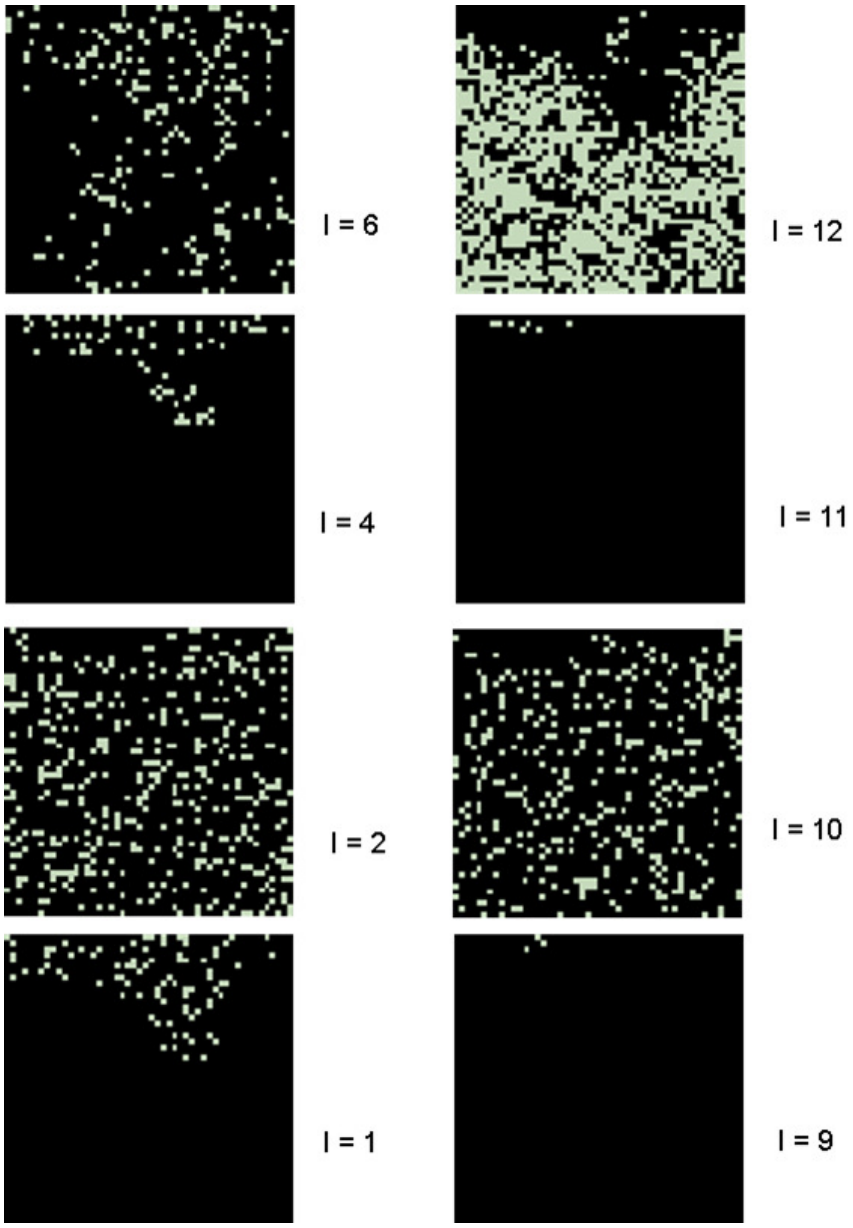

Figure S3. Examples of nanometer scale image areas used for generation of the statistical distributions of the TrkB membrane protein receptor dimers and clusters. The image sizes are equal to 283.5×283.5 nm^2.

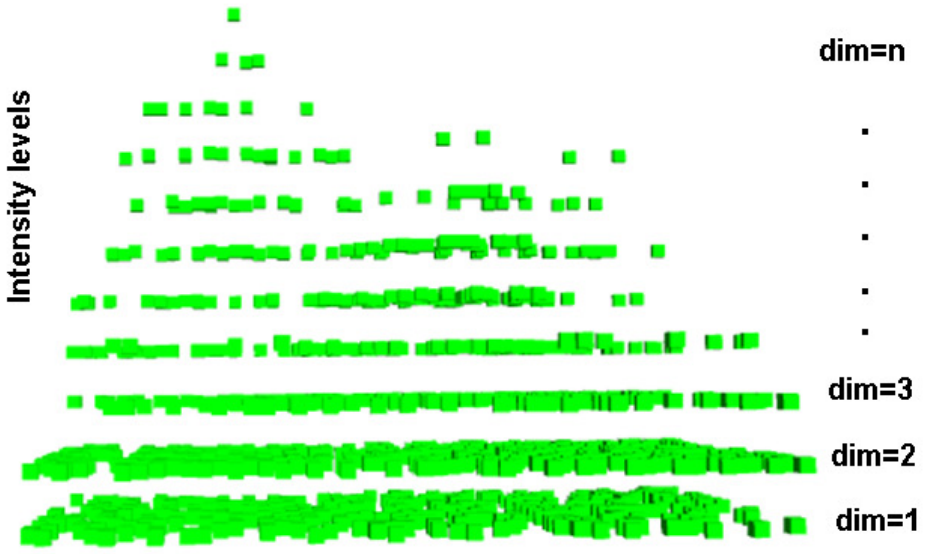

Figure S4. Example of quantification of the dimeric TrkB protein receptors using the fluorescent intensity levels from a selected area (283.5×283.5 nm^2) of a STED image. Every fluorescent pixel contains a single dimer of the TrkB membrane receptor protein. The pixel dimension is 5.67×5.67 nm^2 in the magnified *Huygens* deconvoluted gated STED images.

Determination of protein cluster phases from super-resolution STED images

Table S1

Results of statistical analysis of membrane protein TrkB receptor nanoclustering.

Condition	Total number of dimers and clusters / Distinct nanodomain sizes	Oligomeric states of TrkB receptor (average data calibrated to 100% total)*			
		$n=1$	$n=2$	$n=3$	$n=4$
1. Before incubation with DHA	251101 / 1243	61% ± 1%	17% ± 1%	7% ± 1%	4% ± 1%
2. After incubation with DHA	165097 / 973	65% ± 1%	16% ± 1%	6% ± 1%	3% ± 1%

*Frequency of clustering events for statistical results shown in Fig. 5. The isolated TrkB receptor dimers (or couples of monomers) were distinguished from the higher-order oligomers through statistical analysis of the surface area occupied by the membrane protein nanoclusters (Fig. 4, Fig. S2). Every pixel in the magnified super-resolution images may be occupied by a single dimeric receptor ($n=1$) or by one or two monomeric proteins. The sum of the percentages of the various monomeric, dimeric and oligomeric states of the TrkB receptor equals 100% in both cases. However, the absolute numbers of the TrkB receptor clusters, which are present in the cellular membranes, differ for each condition and demonstrate the effect of DHA on the dissolution of the TrkB receptor cluster phases. The total number of distinct clusters significantly decreases as a result of the DHA treatment. Upon DHA addition, the number of individual dimers and/or monomers (resp. the number of single pixels) increases at the expense of the oligomeric states.

Determination of protein domain gyration radius from crystallographic data

The structural parameters of the extracellular segment of the human neurotrophin receptor dimer were used for estimation of the domain gyration radius. The *DS Viewer* software for protein modelling (*Accelrys*) was employed for calculation of the gyration radius of the extracellular portion of the membrane receptor dimer based on the available X-ray crystallographic data (PDB code: 2IFG).

The *DS Viewer* software yielded a radius of gyration r= 44.8 Å.

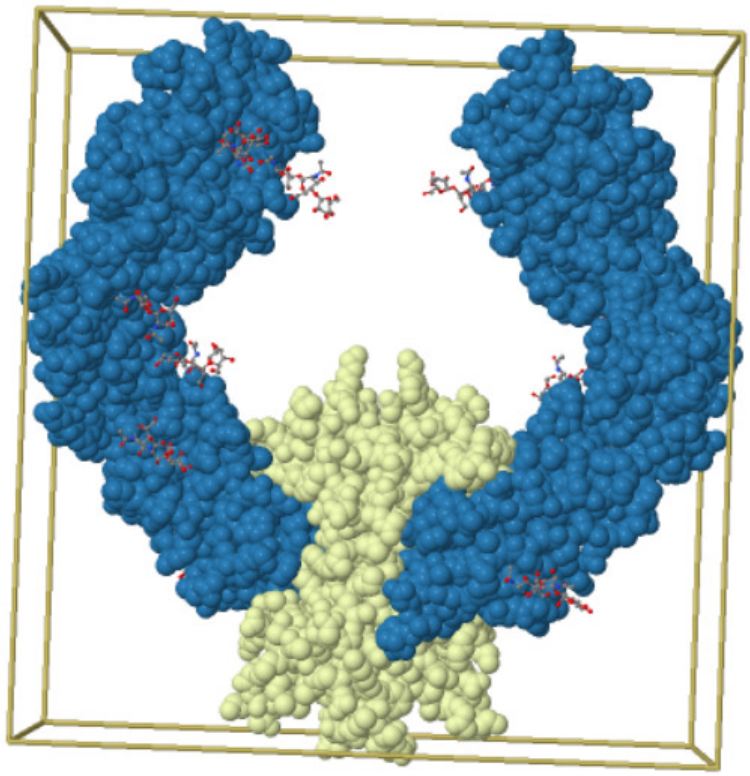

Figure S5. Three-dimensional view of the extracellular domain (blue colour) of the Trk membrane receptor dimer formed upon binding of a neurotrophin ligand (light green colour). The X-ray crystallographic data were taken from the PDB file **2IFG** published for a member of the human neurotrophin receptor family (PDB source from He and Garcia, 2007).

III. Supplementary References

1. Vicidomini, G.; Moneron, G.; Han, K.Y.; Westphal, V.; Ta, H.; Reuss, M.; Engelhardt, J.; Eggeling, C.; Hell, S.W. Sharper low-power STED nanoscopy by time gating. *Nature methods* **2011**, *8*, 571-573, doi:10.1038/nmeth.1624.

2. Hell, S.W., Wichmann, J. Breaking the diffraction resolution limit by stimulated emission: stimulated-emission-depletion fluorescence microscopy. *Optics letters* **1994**, *19*, 780-782.

3. Willig, K. I.; Harke, B.; Medda, R., Hell, S.W. STED microscopy with continuous wave beams. *Nature methods* **2007**, *4*, 915-918, doi:10.1038/nmeth1108.

4. Pinot, M.; Vanni, S.; Pagnotta, S.; Lacas-Gervais, S.; Payet, L.A.; Ferreira, T.; Gautier, R.; Goud, B.; Antonny, B.; Barelli, H. Polyunsaturated phospholipids facilitate membrane deformation and fission by endocytic proteins. *Science* **2014**, *345*, 693-697.

5. Deng, Y.; Almsherqi, Z.A.; Shui, G.; Wenk, M.R.; Kohlwein, S.D. Docosapentaenoic acid (DPA) is a critical determinant of cubic membrane formation in *amoeba Chaos* mitochondria. *FASEB J.* **2009**, *23*, 2866-2871.

6. Shaikh, S.R.; Cherezov, V.; Caffrey, M.; Stillwell, W.; Wassall, S.R. Interaction of cholesterol with a docosahexaenoic acid-containing phosphatidylethanolamine: Trigger for microdomain/raft formation? *Biochemistry* **2003***, 42*, 12028-12037.

7. Brzustowicz, M.R.; Cherezov, V.; Zerouga, M.; Caffrey, M.; Stillwell, W.; Wassall, S.R. Controlling membrane cholesterol content. A role for polyunsaturated (docosahexaenoate) phospholipids. *Biochemistry* **2002***, 41*, 12509-12519.

8. Konyakhina, T. M.; Feigenson, G. W. Phase diagram of a polyunsaturated lipid mixture: Brain sphingomyelin/1-stearoyl-2-docosahexaenoyl-sn-glycero-3-phosphocholine/cholesterol. *Biochim. Biophys. Acta-Biomembranes* **2016***, 1858*, 153-161.

9. Fabelo, N.; Martin, V.; Santpere, G.; Marin, R.; Torrent, L.; Ferrer, I.; Diaz, M. Severe alterations in lipid composition of frontal cortex lipid rafts from Parkinson's disease and incidental Parkinson's disease. *Molec. Med.* **2011***, 17*, 1107-1118.

10. Fabelo, N.; Martin, V.; Marin, R.; Moreno, D.; Ferrer, I.; Diaz, M. Altered lipid composition in cortical lipid rafts occurs at early stages of sporadic Alzheimer's disease and facilitates APP/BACE1 interactions. *Neurobiol. Aging* **2014***, 35*, 1801-1812.

11. Pan, Y., Khalil, H., Nicolazzo, J.A. The impact of docosahexaenoic acid on Alzheimer's disease: Is there a role of the blood-brain barrier? *Curr. Clin. Pharmacol*. **2015**,*10*, 222-241.

12. Grimm, M.O.W.; Kuchenbecker, J.; Grosgen, S.; Burg, V.K.; Hundsdorfer, B.; Rothhaar, T.L.; Friess, P.; de Wilde, M.C.; Broersen, L.M.; Penke, B.; Peter, M.; Vigh, L.; Grimm, H.S.; Hartmann, T. Docosahexaenoic acid reduces amyloid beta production *via* multiple pleiotropic mechanisms. *J .Biol. Chem.* **2011***, 286*, 14028-14039.

13. Teng, E.; Taylor, K.; Bilousova, T.; Weiland, D.; Pham, T.; Zuo, X.H. ; Yang, F.S.; Chen, P.P.; Glabe, C.G.; Takacs, A.; Hoffman, D.R.; Frautschy, S.A.; Cole, G.M. Dietary DHA supplementation in an APP/PS1 transgenic rat model of AD reduces behavioral and Aβ pathology and modulates Aβ oligomerization. *Neurobiol. Disease,* **2015***, 82*, 552-560.

14. Tanaka, K.; Farooqui, A.A.; Siddiqi, N.J.; Alhomida, A.S.; Ong, W.Y. Effects of docosahexaenoic acid on neurotransmission. *Biomolec. & Therapeut.* **2012***, 20*, 152-157.

15. Emendato, A.; Spadaccini, R.; De Santis, A.; Guerrini, R.; D'Errico, G.; Picone, D. Preferential interaction of the Alzheimer peptide Aβ-(1-42) with omega-3-containing lipid bilayers: structure and interaction studies. *FEBS Lett.* **2016***, 590*, 582-591.

16. Shaikh, S.R.; Kinnun, J.J.; Leng, X.L.; Williams, J.A.; Wassall, S.R. How polyunsaturated fatty acids modify molecular organization in membranes: Insight from NMR studies of model systems. *Biochim. Biophys. Acta-Biomembranes* **2015***, 1848*, 211-219.

17. Pereira, D.B.; Chao, M. V. The tyrosine kinase Fyn determines the localization of TrkB receptors in lipid rafts. *J. Neurosci.* **2007***, 27*, 4859-4869.

18. He, X., Garcia, K.C. Structure of the extracellular segment of human TrkA in complex with nerve growth factor. *Neuron* **2007***, 53*, 25-38.

19. Géral, C., Angelova, A., Angelov, B., Nicolas, V., Lesieur, S., Chapter 11: Multicompartment lipid nanocarriers for targeting of cells expressing brain receptors, In "Self-Assembled Supramolecular Architectures: Lyotropic Liquid Crystals". Garti, N.,

Somasundaran, P, Mezzenga, R. (Editors), John Wiley & Sons, Inc., New Jersey, 2012, pp. 319-355.

20. Encinas, M.; Iglesias, M.; Liu, Y.H.; Wang, H.Y.; Muhaisen, A.; Cen,a V.; Gallego, C.; Comella, J.X. Sequential treatment of SH-SY5Y cells with retinoic acid and brain-derived neurotrophic factor gives rise to fully differentiated, neurotrophic factor-dependent, human neuron-like cells. *J. Neurochem*. **2000**, *75*, 991-1003.

21. Guerzoni, L.P.B., Nicolas, V., Angelova, A. *In vitro* modulation of TrkB receptor signaling upon sequential delivery of curcumin-DHA loaded carriers towards promoting neuronal survival. *Pharmaceutical Research* **2017**, *34*, 492-505.